


Structural, mechanical and tribological properties of WCTiN coatings produced by HiPIMS

Proc IMechE Part B:
J Engineering Manufacture
1–10
© IMechE 2023
Article reuse guidelines:
sagepub.com/journals-permissions
DOI: 10.1177/09544054231174976
journals.sagepub.com/home/pib


J Sanches¹, F Ferreira^{1,2}, F Fernandes^{1,3}, A Cavaleiro^{1,2}
and R Serra¹ [AQ: 1][AQ: 2]

Abstract

Wear can be decreased by applying protective multi-element thin films on the surface of mechanical components (e.g., cutting tools and brake discs). The current study examines how substrate polarisation voltage affects the structural-mechanical relationships of WTiCN thin films made using a combination of HiPIMS and DCMS reactive sputtering. A chemical and structural study of the coatings conducted using EDS and XRD reveals the development of a composite phase structure. Additionally, the microstructure and morphology of the coating, as revealed by SEM and AFM, shows that defect-free surfaces are possible to obtain. Then, sliding (scratch and pin-on-disk) and indentation (nano-indentation) tests are used to examine the films' mechanical characteristics (hardness, adhesion, friction coefficient and wear rate). It shows that substrate polarisation voltage of -60 V must be used to generate surfaces that are resistant to wear. The reason for this is the ideal levels of tungsten concentration (19 at.%), root mean square surface roughness (4.5 nm) and hardness (29 GPa) have been reached.

Keywords

WCTiN, HiPIMS, DOMS, tribology, wear resistance

Date received: 30 June 2022; accepted: 22 April 2023

Introduction

TiN thin films, which were developed starting in the 1980s, are the first generation of hard protective coatings.^{1–3} Some elements, including Cr, Mo, V, Nb and W (elements of the IVB, VB and VIB columns in the periodic table), were added to these films to increase their hardness and enhance the tribological performance.^{4–7} The other qualified possibilities are Al and Si.^{8,9} Adding carbon to TiN films, according to experts,^{10,11} might be a potential option for application in mechanical components, such as cutting tools and brake discs. As a result, multi-element coatings may be good choice to meet demanding mechanical requirements, namely high and stable coefficient of friction (CoF) and low specific wear rate. Some attempts have been undertaken to create tungsten nitride/carbide coatings since tungsten-based compounds are among the hardest materials in nature.^{12–15} Considering this, it is expected that W-Ti-C-N thin films may be among the best options for providing appropriate tribological performance. However, the use of these ceramic materials has its own restrictions. Contrary to thin metallic films,

these materials have good hardness, yet the fracture toughness and substrate adherence are key problems that might diminish the tribological capabilities.^{16,17} Wear-resistant coatings with adapted toughness and adhesion can be ensured by using defect-free, compact films with nano-sized grains and interlayers.^{18–20}

Physical vapour deposition (PVD) technologies are the most effective among the vapour deposition techniques (physical or chemical) to get good quality coatings. Sputtering is more popular than other PVD

¹Department of Mechanical Engineering, University of Coimbra, CEMMPRE – Centre for Mechanical Engineering Materials and Processes, Coimbra, Portugal

²LED&Mat-IPN, Instituto Pedro Nunes, Laboratório de Ensaios Desgaste e Materiais, Coimbra, Portugal

³Mechanical Department, ISEP, Porto School of Engineering, Porto, Portugal

Corresponding author:

R Serra, Department of Mechanical Engineering, CEMMPRE – Centre for Mechanical Engineering Materials and Processes, University of Coimbra, Rua Luís Reis Santos, Coimbra, 3030-788, Portugal.
Email: ricardo.serra@dem.uc.pt

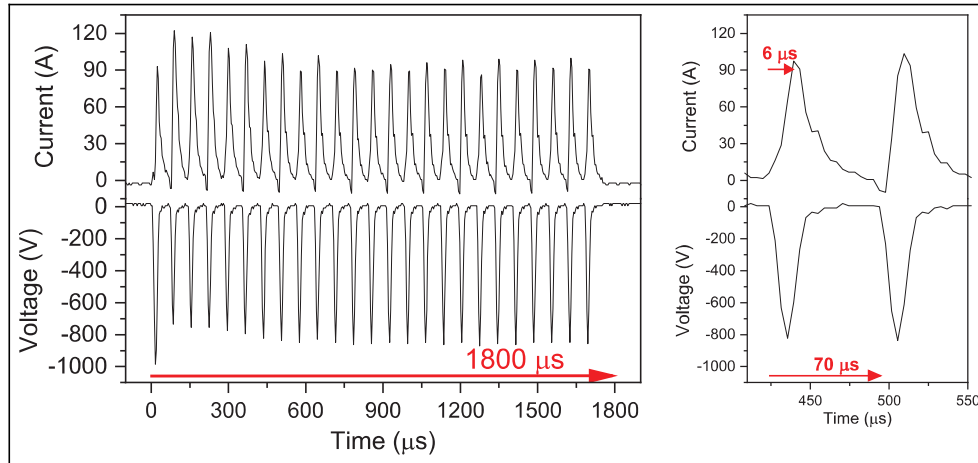


Figure 1. Target voltage and target current waveforms obtained during the sputtering of titanium target in Ar/N₂ atmosphere by DOMS.

processes, like arc and evaporation methods, because it can simultaneously meet industrial conditions (high deposition rate and low temperature/energy consumption) and technological aspects (high surface uniformity without defects like macroparticles).^{21–24} Direct current magnetron sputtering (DCMS) has so far been the common setup used for depositions. However, it has its own limitations, like reduced plasma ionisation and energetic particles received at the substrate surface.^{20,25} To overcome these limitations, high power impulse magnetron sputtering (HiPIMS), also known as iPVD (an ionised form of PVD²⁶), was developed. Recently, this technique has been preferred because of higher particle mobility at the substrate surface, and as a result, higher coating densities (without pores and open boundaries) are obtained. Generally, homogenous nanostructured films are formed, and these features are of great importance in the mechanical responses of materials.²⁷ Process variables that impact the quality of the films' structure during sputtering deposition include the substrate polarisation voltage,^{28,29} peak power density,^{30,31} type and content of the reactive and plasma gases,^{32–34} base pressure³⁵ and substrate temperature.^{32,36} As mentioned before, because of the higher particle energies in HiPIMS, the rising substrate temperature is seldom applied in HiPIMS.³⁷ Furthermore, gas properties have been extensively investigated.^{33,34} However, while several studies examine the mechanical characteristics of multi-element (more than three elements) thin films made by HiPIMS,^{27,38} few publications³⁹ have examined the tribological behaviour of multi-element coatings when substrate polarisation voltage changes (parameter crucial to control the energy of ionised particles).

To achieve superior tribological characteristics it is crucial to determine the ideal level of substrate polarisation voltage during HiPIMS operations. Determining the structural-mechanical changes of WTiCN thin films produced by combining HiPIMS and DCMS is the

primary goal of this investigation. The value of the substrate polarisation voltage was varied from 0 to -80 V while the other parameters remained constant. First, the coatings' chemical composition and structure are discussed. Then, topographical and morphological aspects are examined. Additionally, mechanical properties (scratch and pin-on-disk tests) are analysed. A thorough description of adhesion and wear properties is finally provided.

Experimental procedure

The WTiN thin films were deposited in co-sputtering using a DCMS power supply (ENI RPG50) connected to the tungsten carbide (WC) compound target and a HiPIMS power supply (Cypirum™ plasma generator, Zpulsor Inc) working in deep oscillation magnetron sputtering mode (DOMS), connected to the titanium (Ti) target.^{29,40} Both target dimensions were 150×150 mm with 8 mm thickness. DOMS was already proven to be reliable in producing TiN-based coatings.^{41–43} For this work, DOMS 1800 μs pulse was subdivided in 25 oscillations of 6 μs on-time and 70 μs period (Figure 1) was used, resulting in a duty cycle of 1.8%. The WTiN films were prepared using increasing negative substrate polarisation, ranging from 0 up to -80 V, to verify their influence on the films mechanical and tribology properties. M2 steel substrates with a geometry of 25 mm diameter and 8 mm height were used for tribological tests, and silicon wafers were used for morphology, structure and chemical composition analysis. The substrate distanced from both targets 80 mm, and the substrate holder rotated at 23.5 rpm.

Before the depositions, a base vacuum pressure of 1.8×10^{-4} Pa was achieved and, before the film deposition, a cleaning/etching step was performed to the substrates using pulse power unit (350 V at 120 kHz and 1616 ns in Ar atmosphere at 0.4 Pa) for 60 min. After the cleaning step, an interlayer composed of Ti (10 min

Table 1. Deposition parameters used for the WCTiN films.

Substrate bias (V)	Ti, DOMS			WC, DCMS	
	Frequency (Hz)	Peak voltage (V)	Peak current (A)	Voltage (V)	Current (A)
0	100	1112	55	435	1.6
-40	100	1118	54	444	1.6
-60	93	1167	55	458	1.5
-80	87	1150	55	450	1.6

Table 2. Chemical composition of the WCTiN samples obtained by EDS.

Substrate bias (V)	O (at.%)	Ti (at.%)	W (at.%)	C (at.%)	N (at.%)
0	3.5	13.8	17.4	20.4	44.8
-40	2.0	13.9	18.5	19.9	45.8
-60	2.5	14.2	19.2	18.2	45.9
-80	2.2	16.8	17.0	16.0	48.0

in Ar atmosphere at 0.4 Pa with Ti target) and a TiN support layer (10 min with 0.4 Pa Ar + 0.4 Pa of N₂ again with Ti target) was performed under DOMS regime at 700 W time average power. For the depositions, both targets were operated at 700 W, with 0.8 Pa of total pressure for 50 min, adjusting the polarisation level according to the parameters of Table 1.

Scanning electron microscopy (SEM) (Quanta 400FEG ESEM equipment) was used to obtain the thickness and morphology of the films using a 2 keV electron beam for both cross-section and surface micrographs. The film's composition was obtained by energy dispersive spectroscopy (EDS) in the same equipment. The coating's surface morphology was acquired by atomic force microscopy (AFM) on a Bruker Innova system, performing the measurements in tapping mode with a silicon tip with tip radius lower than 8 nm. The scan size was $3 \times 3 \mu\text{m}$, and the roughness measurements were performed after image mean plane and polynomial levelling. X-ray diffraction measurements were performed on a PANalytical X'Pert PRO MPD diffractometer with Cu $K\alpha$ radiation at 45 kV and 40 mA. The system uses parallel beam in θ - 2θ geometry, with incident beam optics constituted by a hybrid monochromator with a Cu W/Si mirror and a double crystal Ge (220). In the path of the diffracted beam was mounted a parallel plate collimator (0.7°) and a Soller slit (0.004°). A PIXcel detector in receiving slit mode was used for X-ray collection.

Hardness and reduced Young's modulus of the films were measured in nano-indentation equipment (Micro Materials Nano Tester) equipped with a Berkovich diamond indenter. The hardness was evaluated from load-displacement curves using the depth-sensing method, performing 16 hardness measurements in each specimen with 5 mN load, ensuring that the indentation depth is lower than 10% of the coating's thickness. The coefficient of friction (CoF) measurements were obtained

from a homemade pin-on-disk apparatus tested against 10 mm steel balls (AISI 52100) with 5 N load for 4000 cycles at 0.1 m/s. All the measurements were performed at laboratory conditions (22°C and 40% humidity). Specific wear rate was then calculated using a 2D profilometer (Mitutoyo Surf test SJ-500) measuring the wear on three equally distant profile points of the worn tracks resulted from the previously mentioned pin-on-disk test. Surface and composition analysis after pin-on-disk tests were performed in SEM Hitachi model SU3800 coupled with Bruker Quantax Compact EDS detector. Scratch tester using an automatic scratch tester, CSEM – REVETEST, fitted with a Rockwell 'C' diamond-tipped indenter with a spherical tip radius of 100 μm was used to evaluate the adhesion of the films. In the experiments, the normal load increased linearly from 0 to 60 N with a speed of 10 mm/min. Samples and indenter were ethanol cleaned before testing, and an optical microscope was used to quantify the adhesive properties of the thin films.

Results

Table 2 presents the element concentration of the WTiCN thin films extracted from EDS analysis. As can be seen, by increasing substrate polarisation potential, both metallic percentages (W + Ti) and nitrogen content in the coatings rise gradually. In contrast, carbon content gets lower values and oxygen (usual impurity in PVD productions^{20,32}) appears only in low amounts (below 3.5 at.%). Hence, the metals to nonmetals ratio increases with substrate polarisation voltage increase (from 45 to 51%). It must be mentioned that other impurities (like Ar, which can be in thin films in extremely low amounts⁸) contents are lower than 0.2 at.%. These trends can be explained by the particle's energy and weight.²⁵ At higher levels of substrate

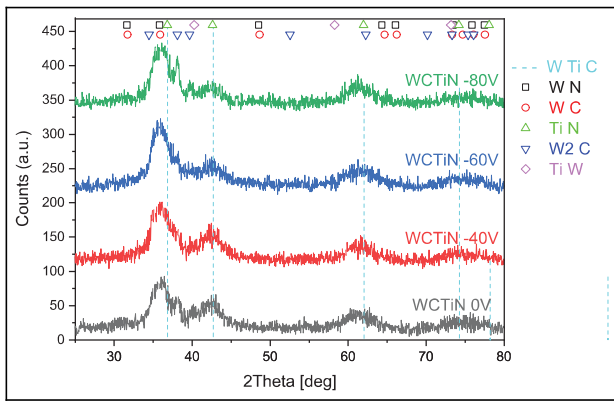


Figure 2. X-ray diffraction patterns of the WCTiN films prepared by DOMS.

polarisation voltage, particles with higher weights (W and Ti ions/atoms) diffused and deposited to the coating more efficiently and the nitrogen can substitute the carbon in the growing layer. Nitrogen amount in the thin films is higher than carbon, and on the other hand, nitrogen content rises while carbon content becomes lower. As a result, nitride compounds content can grow gradually while carbide compounds amount reduces significantly.

The X-ray diffraction results patterns of all the films are shown in Figure 2. Hybrid/composite phase structures (crystalline phases plus amorphous phase) are obtained. Adding to it, the amorphous phase is the major phase in all the thin films, while some low-content nano-crystalline phases can be observed. A high content of the amorphous phase in the thin films produced by co-sputtering in the presence of a high N ratio ($P_{N_2}/P_{Ar} = 0.5$) is usual.^{4,13} Moreover, crystalline

phases can be attributed to WTiC (ICDD no 00-020-1309), TiW (ICDD no 00-049-1440), WC (ICDD no 00-002-1055), WN (ICDD no 00-025-1256), TiN (ICDD no 00-006-0642), W_2C (ICDD no 00-002-1134). Peak broadening can be assigned to overlapping the XRD patterns of the abovementioned phases and nanocrystalline structures. However, since the chemical composition shows all the elements, the films formed can be considered WCTiN.

The surface SEM micrographs, together with the respective insets cross-section micrographs of the WCTiN films, are shown in Figure 3. The micrographs have similar cauliflower-like surface morphology for the four films, without any substantial variation between them. The cross-section micrographs also show similar dense microstructure for the four films. The thickness of the four films is constant at around $1\ \mu\text{m}$. The thin Ti/TiN interlayer (120 nm) used for adhesion and support is also visible in cross-section micrographs.

The constant cauliflower-like surface morphology agrees with the AFM measurements (images not shown). Their surface height ranges from $-18\ \text{nm}$ up to $23\ \text{nm}$ in all four samples, and the root mean square surface roughness (S_q) values of 5.0, 5.7, 4.5 and 5.1 nm, respectively, for 0, -40 , -60 and $-80\ \text{V}$ of substrate polarisation.

The surface morphology results have no defined tendency that can be attributed to the substrate polarisation used in this work. However, the results are characteristic of films deposited by HiPIMS (dense films) but with some influence of shadow effects during film growth (cauliflower surface). In general, the polarisation applied to the substrates does not influence their morphology and structure.

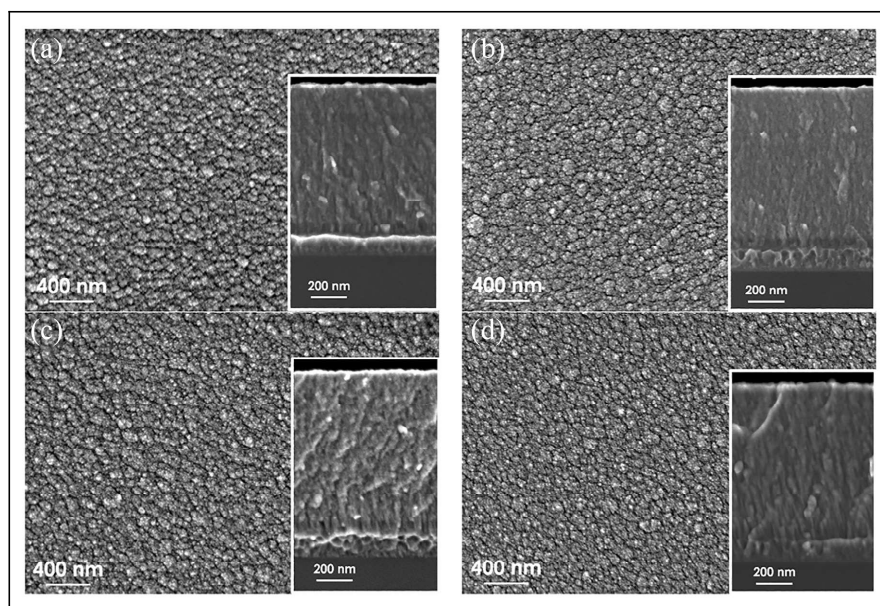


Figure 3. SEM surface micrographs and cross-section inset micrographs of WCTiN films prepared with substrate polarisation of: (a) 0 V, (b) $-40\ \text{V}$, (c) $-60\ \text{V}$ and (d) $-80\ \text{V}$.

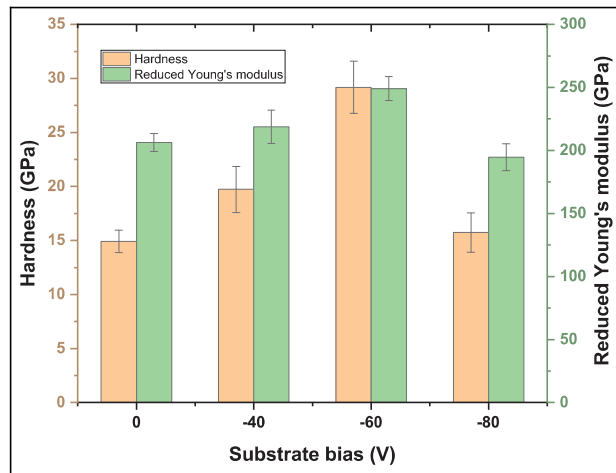


Figure 4. Hardness and Young's Modulus of the WCTiN films prepared by DOMS.

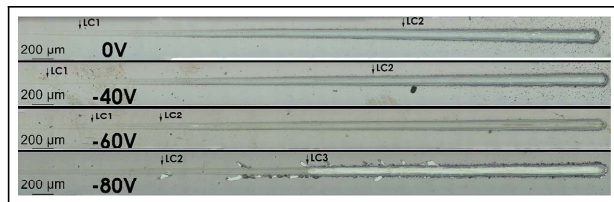


Figure 5. Scratch test photos for WCTiN done up to 60 N with a 10 N/mm applied force.

The hardness and reduced Young's modulus of the films are presented in Figure 4. The graph reveals an increase of both parameters with the increase of substrate polarisation from 0 until -60 V, in accordance with the literature.⁴⁴ The highest value is obtained for the sample with substrate polarisation of -60 V, with a hardness of 29 GPa, starting from 15 GPa for 0 V of substrate polarisation. This high value is already superior to W-C-Ti coating, which typically ranges from 15 to 17 GPa.⁴⁵ The Young's Modulus values for the same films are also increasing, starting above 200 until 250 GPa. In these films, the mechanical parameters have a relation with the increase of bombarding energy, i.e., the more negative substrate polarisation increases the surface bombardment increasing the respective compactness of the films and increasing the respective mechanical properties. Substrate polarisation at -80 V shows a drop of both hardness and Young's Modulus values back to 15 and 200 GPa, respectively.

Optical images of scratch tests done for the four samples are shown in Figure 5. For the WCTiN films deposited with 0 V substrate polarisation LC1 type failure starts at 6.6 N of load. This type of failure extends and becomes more noticeable at 11.8 N, where visible vertical cracks become prominent, reaching the scratch sidewalls. At 37.4 N of load, LC2 type failure begins with delamination points of the thin film. When -40 V

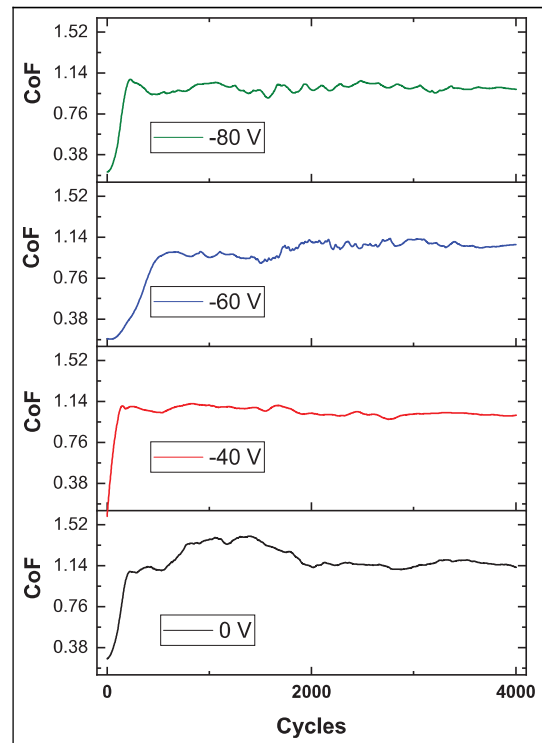


Figure 6. Coefficient of friction for the WCTiN thin films. Pin-on-disk test ran for 4000 cycles.

of substrate polarisation is used during the deposition of the WCTiN film, the LC1 failure starts earlier, at 3.4 N, showing propagation like the 0 V sample. Likewise, the LC2 type of failure occurs earlier at 34.8 N. The WCTiN film deposited with -60 V of substrate polarisation has a latter LC1 failure at 9.4 N of load but earlier LC2 failure at 17.2 N of load. Despite this earlier LC2 failure of the film, the scratch track has less cracks with only seemingly random LC2 type failures that do not proportionally increase in number with increasing applied load, contrary to previous samples.

The scratch result for the WCTiN film prepared with -80 V starts with a very visible LC2 failure point at 14.2 N of load, later developing and turning into an LC3 type failure at 28.8 N of load. Such failure is in conformity with adhesion failure and backs up the hardness and Young's Modulus drop for this sample (Figure 4). This behaviour is attributed to a film compromised due to internal residual stress forces, as seen in similar materials.⁴⁶ These residual stress forces hinder the adhesion of the WCTiN thin film to the substrate steel disk, limiting their application.

The CoF of the WCTiN films prepared in this work appears in Figure 6. The CoF results have similar values in the steady state zone of the measurements, between 1.0 and 1.2, after 500 cycles mark. There are some differences during the running-in period between the samples. For the 0 V WCTiN film, after the initial 100 cycles of fast increase of CoF attributed to the

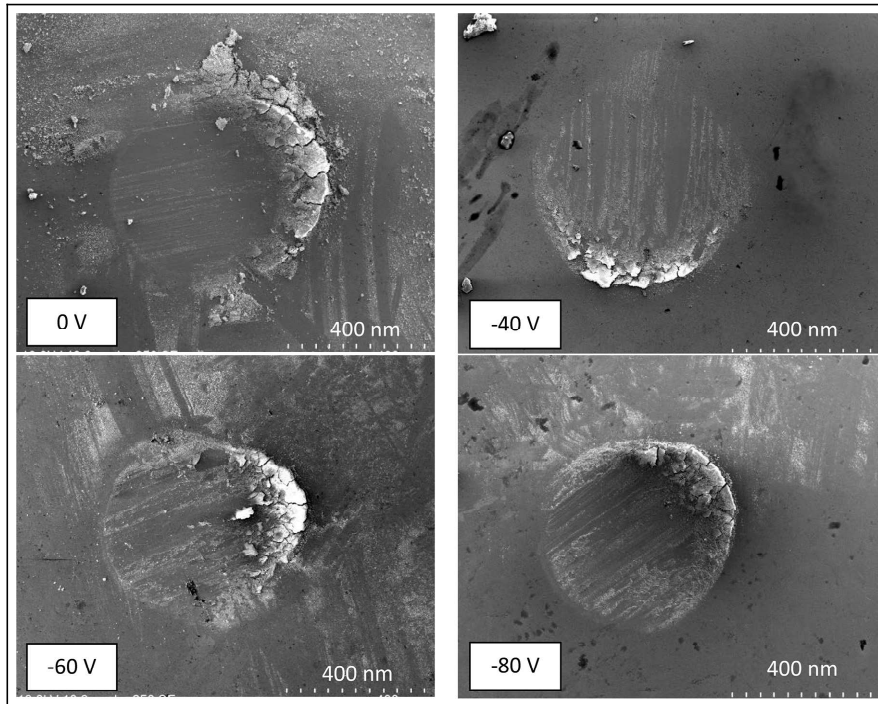


Figure 7. SEM of 10 mm steel ball (AISI 52100) used for the 4000 cycles pin-on-disk tribology testing.

running-in period, slightly above 1.4 CoF value is measured before reaching the steady state between 500 and 2000 cycles. Another difference was obtained for the WCTiN film prepared with -60 V of substrate polarisation, where longer running-in occurred until 500 cycles.

The SEM micrographs of the pin after pin-on-disk tests are shown in Figure 7. The contact point of the pins shows an accumulation of wear debris around the edges of the worn area. There are also signs of material inclusions from the coating in the worn area. The difference between the contact area between 0 and -40 V samples, as compared with -60 and -80 V, is that the latter two are the ones with the smaller worn area. Moreover, the pin used for WCTiN prepared with 0 V of substrate polarisation shows a smaller amount of material inclusion.

The SEM micrographs of the wear tracks on the WCTiN films after the pin-on-disk tests are shown in Figure 8. The amount of material embedded in the wear track during the testing increases with the increase of negative substrate polarisation. The WCTiN film prepared with 0 V of substrate polarisation shows the lowest quantity of embedded debris in the coating. This is the less hard film (compared with the rest of the samples prepared for this work), and, as a result, particles worn from the pin must be low. The other films are significantly harder, which results in a higher capability of pin wear with respective particles being released and embedded in the coatings. As seen in Figure 7, this also results in higher quantity of material transfer to the respective pins.

Further examination was conducted with the composition of the worn areas and debris on both pin and coating (Tables 3 and 4, respectively), confirming that material transfer had occurred mutually. Material transfer from the coating to the pin is confirmed by the composition EDS results measured in those areas, Table 3, since W, Ti, C and N traces are obtained. The results also show that the transferred material is oxidised, that is, a higher quantity of O element is obtained in the debris. The composition of the unused pin is also shown in Table 3 for comparison, and only Fe, C and Cr together with residual O is measured.

Table 4 shows the composition results of the worn area of the WCTiN coatings after pin-on-disk testing. The composition analysed in the coating shows similar but inversed behaviour. In this case, in the debris area the film composition shows a reduction of elements quantity (W, Ti, C and N) together with signals from the pin (Fe) and increased O element signal, resulting from oxidation. In the worn areas, the film composition appears closer to the initial unused film without the oxygen signal. In this last case, we can conclude that the film maintains the composition and does not show signs of surface oxidation resulting from the pin-on-disk testing.

From the results already presented, two types of wear mechanisms can be suggested. The sample prepared at 0 V has fewer debris embedded in the film worn track. The hardness of this film is lower (compared with the other samples studied here), and as a result, pin debris removal and respective embedding in the coating is not promoted. The wear occurs simply by

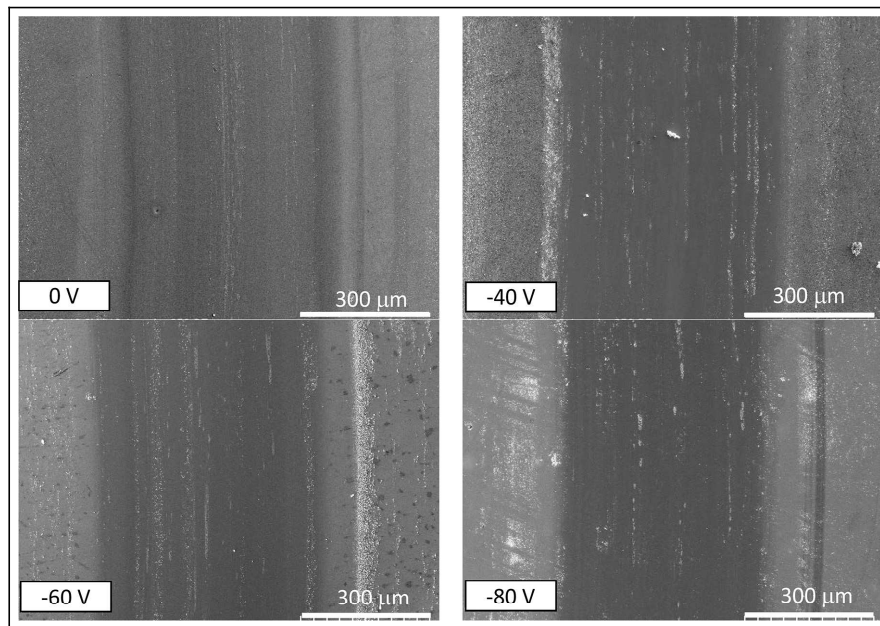


Figure 8. SEM of wear tracks after the 4000 cycles pin-on-disk tribology testing.

Table 3. Composition obtained by EDS measurements in the pins worn after pin-on-disk testing of the WCTiN films with changing substrate polarisation.

Element	Pin	0 V		−40 V		−60 V		−80 V	
		Transfer	Worn	Transfer	Worn	Transfer	Worn	Transfer	Worn
W	–	4.9	–	5.8	–	9.9	–	6.8	–
C	14.6	8.3	9.4	9.3	9.9	11.3	9.6	12.0	11.6
Ti	–	5.7	–	5.8	–	9.0	–	7.1	–
N	–	2.8	–	2.8	–	4.5	–	1.5	–
Cr	1.2	–	1.2	–	1.6	–	1.5	–	1.0
Fe	81.4	38.8	89.5	40.0	88.5	3.7	88.9	21.6	87.4
O	2.9	39.6	–	36.2	–	61.5	–	51.0	–

Pin represents the composition reference on the clean and unused pin; *transfer* to composition measured on particles in the contact point; and *worn* to the worn contact point of the pin.

Table 4. Composition obtained by EDS measured in the wear track after pin-on-disk tests for WCTiN films prepared with changing substrate polarisation.

Element	WCTiN film	0 V		−40 V		−60 V		−80 V	
		Debris	Worn	Debris	Worn	Debris	Worn	Debris	Worn
W	15.5	12.5	13.7	10.9	16.5	12.1	15.6	12.4	13.4
C	28.5	16.2	20.7	11.2	20.1	17.5	25.8	20.5	23.0
Ti	11.2	15.7	18.2	11.6	17.8	9.1	13.1	11.7	16.8
N	39.2	24.6	40.8	10.1	40.2	16.4	40.6	32.1	41.9
Fe	1.9	2.5	3.3	7.7	2.3	1.2	2.9	1.5	2.1
O	3.8	28.5	3.3	48.5	3.2	43.7	2.1	21.7	2.9

WCTiN film represents the composition reference on clean and unused WCTiN coating; *debris* corresponds to composition measured on particles in the wear track; and *worn* to the wear track of the coating.

pin and coating erosion during testing. The less hard film withstands higher surface wear during testing. The samples prepared at −40, −60 and −80 V have a higher

amount of embedded pin debris in the worn area of the track. The wear mechanism in these samples corresponds to hard coating wearing the pin and respective

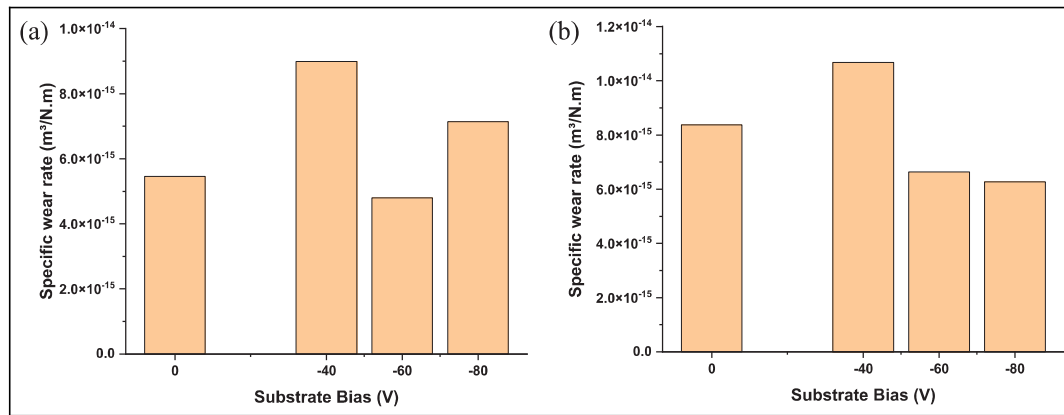


Figure 9. Specific wear rate for the WCTiN thin films after 4000 cycles for (a) pin and (b) WCTiN coating.

released pin debris embedded into the coating. This further promotes the wear of these coatings.

Graphs of specific wear rates calculated for the pin and for the coating are displayed in Figure 9. The results confirm the two types of wear mechanisms. In the samples with substrate polarisation of 0 and -40 V, both pin and coating present higher specific wear rates. The samples with substrate polarisation of -60 and -80 V have lower specific wear rates. The pin specific wear rate, Figure 9(a), on the other hand, for WCTiN prepared with -80 V of substrate polarisation confirms the coating instability, presenting higher specific wear values due to its poor adhesion on the substrate and faster degradation.

In this work, the WCTiN films with -60 V of substrate polarisation are the most stable and with the best properties for further investigation. The results show that the wear mechanism consists in coating and pin wear with the formation of debris that add to the pin (material transfer) and get embedded into the coatings. This process shows faster coating degradation and higher pin wear.

The increase of the negative substrate polarisation, together with the HiPIMS/DOMS sputtering deposition process, leads to an increase of the bombarding energy during film growth up to the point of adhesion failure. From the deposition conditions used in this work, -80 V was the point where the film peeling off started to occur, limiting the testing and film performance.

Conclusion

Thin WCTiN films were successfully deposited via co-sputtering of tungsten carbide target with DCMS and titanium with HiPIMS in a reactive nitrogen environment. According to chemical composition investigation, the coatings' metallic percentages (W + Ti) and nitrogen content steadily increase as substrate polarisation potential rises. In contrast, the carbon

concentration is decreased, and the oxygen content is low (less than 3.5 at.%). As a result, the ratio of metals to nonmetals rises as substrate polarisation voltage raises (from 45 to 51%). The XRD analyses reveal the formation of hybrid/composite phase structures (crystalline phases plus amorphous phase), regardless of substrate polarisation voltage. Furthermore, the film microstructure is also not affected by the rising of the substrate polarisation voltage. The developed WCTiN films in this work present a very dense microstructure.

The mechanical and tribological properties of the WCTiN films are clearly influenced by the change in the substrate polarisation voltage. Less negative substrate polarisation has the lowest hardness and Young's modulus. The worse performing sample is the -40 V, with lower adhesion (earlier failure seen in Figure 5) and high specific wear rate (the highest values, Figure 9), even if it is 33% harder than the 0 V sample. The 0 V sample claims the lowest harness compared to all others. The -80 V sample has the most unstable results. The adhesion is the worst, with complete early delamination, and hardness is also strongly reduced. Still, CoF maintains similar values and has the lowest specific wear rate (on par with the -60 V sample).

The best-performing film was the one prepared with -60 V of substrate polarisation. This film has the highest hardness of 29 GPa (Figure 4), surpassing other W-C-Ti based coatings, which are typically around 15–17 GPa. The sample has good adhesion and low specific wear rate (around $6 \times 10^{-15} \text{ m}^3/\text{N.m}$), together with high and very stable CoF (around 1.14) throughout the entire test. These interesting properties make these WCTiN films good candidates to be used in demanding applications, that is, cutting tools and brake discs.

Declaration of conflicting interests


The author(s) declared no potential conflicts of interest with respect to the research, authorship, and/or publication of this article.

Funding

The author(s) disclosed receipt of the following financial support for the research, authorship, and/or publication of this article: This research was funded by FEDER funds through the program COMPETE – Programa Operacional Factores de Competitividade – and by national funds through FCT – Fundação para a Ciência e a Tecnologia, under the project UIDB/00285/2020. The paper has been presented at the International Conference on Thin-Film Processing and Application (ICTFPA-2022) organised by Advanced Manufacturing and Materials Processing Group (AdvaMAP).

ORCID iDs

J Sanches  <https://orcid.org/0000-0001-6483-1215>

F Fernandes  <https://orcid.org/0000-0003-4035-3241>

R Serra  <https://orcid.org/0000-0002-9138-4243>

References

- Ramalingam S and Winer WO. Reactively sputtered TiN coatings for tribology for tribological applications. *Thin Solid Films* 1980; 73: 267–274.
- Ma CH, Huang JH and Chen H. Nanohardness of nanocrystalline TiN thin films. *Surf Coat Technol* 2006; 200: 3868–3875.
- Mishra AK, Gopalan H, Hans M, et al. Strategies for damage tolerance enhancement in metal/ceramic thin films: lessons learned from Ti/TiN. *Acta Mater* 2022; 228: 117777.
- Wang Y, He N, Wang C, et al. Microstructure and tribological performance of (AlCrWTiMo)N film controlled by substrate temperature. *Appl Surf Sci* 2022; 574: 151677.
- Herbster M, Döring J, Nohava J, et al. Retrieval study of commercially available knee implant coatings TiN, TiNbN and ZrN on TiAl6V4 and CoCr28Mo6. *J Mech Behav Biomed Mater* 2020; 112: 104034.
- Davies KE, Gan BK, McKenzie DR, et al. Correlation between stress and hardness in pulsed cathodic arc deposited titanium/vanadium nitride alloys. *J Phys Condens Matter* 2004; 16: 7947–7954.
- Musil J and Vlček J. Magnetron sputtering of hard nanocomposite coatings and their properties. *Surf Coatings Technol* 2001; 142–144: 557–566.
- Hsu TW, Greczynski G, Boyd R, et al. Influence of Si content on phase stability and mechanical properties of TiAlSiN films grown by AlSi-HiPIMS/Ti-DCMS co-sputtering. *Surf Coatings Technol* 2021; 427: 127661.
- Sousa VFC, Silva FJG, Lopes H, et al. Wear behavior and machining performance of TiAlSiN-coated tools obtained by dcMS and HiPIMS: a comparative study. *Materials* 2021; 14: 1–18.
- Constable CP, Yarwood J and Münz WD. Raman microscopic studies of PVD hard coatings. *Surf Coat Technol* 1999; 116–119: 155–159.
- Veprek S, Veprek-Hejman MGJ, Karvankova P, et al. Different approaches to superhard coatings and nanocomposites. *Thin Solid Films* 2005; 476: 1–29.
- Armstrong RW. The hardness and strength properties of WC-Co composites. *Materials* 2011; 4: 1287–1308.
- Addonizio ML, Castaldo A, Antonaia A, et al. Influence of process parameters on properties of reactively sputtered tungsten nitride thin films. *J Vac Sci Technol A Vac Surf Film* 2012; 30: 031506.
- Cavaleiro A and Vieira MT. Structure and chemical composition of W-C-Co sputtered films. *Thin Solid Films* 1991; 197: 237–255.
- Pawbake A, Waykar R, Jadhavar A, et al. Wide band gap and conducting tungsten carbide (WC) thin films prepared by hot wire chemical vapor deposition (HW-CVD) method. *Mater Lett* 2016; 183: 315–317.
- Zhang S and Zhang X. Toughness evaluation of hard coatings and thin films. *Thin Solid Films* 2012; 520: 2375–2389.
- Ge FF, Sen HS, Daghbouj N, et al. Toughening mechanisms in V-Si-N coatings. *Mater Des* 2021; 209: 109961.
- Panjan P, Čekada M, Panjan M, et al. Growth defects in PVD hard coatings. *Vacuum* 2009; 84: 209–214.
- Armstrong RW. Hall-Petch analysis of dislocation pile-ups in thin material layers and in nanopolycrystals. *J Mater Res* 2013; 28: 1792–1798.
- Hebbbar Kannur K, Bin Yaqub T, Huminiuc T, et al. Synthesis and structural properties of Mo-S-N sputtered coatings. *Appl Surf Sci* 2020; 527: 146790.
- Gassner M, Rebelo de, Figueiredo M, Schalk N, et al. Energy consumption and material fluxes in hard coating deposition processes. *Surf Coat Technol* 2016; 299: 49–55.
- Brettner E. *Contact modeling of CVD coatings for cutting tools*. Montanuniversität Leoben, 2010. [AQ: 3]
- Boughrara N, Benzarti Z, Khalfallah A, et al. Comparative study on the nanomechanical behavior and physical properties influenced by the epitaxial growth mechanisms of GaN thin films. *Appl Surf Sci* 2022; 579: 152188.
- Wainstein D and Kovalev A. Tribooxidation as a way to improve the wear resistance of cutting tools. *Coatings* 2018; 8: 1–9.
- Bohlmarmark J, Lattemann M, Gudmundsson JT, et al. The ion energy distributions and ion flux composition from a high power impulse magnetron sputtering discharge. *Thin Solid Films* 2006; 515: 1522–1526.
- Gudmundsson JT. The high power impulse magnetron sputtering discharge as an ionized physical vapor deposition tool. *Vacuum* 2010; 84: 1360–1364.
- Xu Y, Li G, Li G, et al. Effect of bias voltage on the growth of super-hard (AlCrTiVZr)N high-entropy alloy nitride films synthesized by high power impulse magnetron sputtering. *Appl Surf Sci* 2021; 564: 1–10.
- Ferreira F, Serra R, Oliveira JC, et al. Effect of peak target power on the properties of Cr thin films sputtered by HiPIMS in deep oscillation magnetron sputtering (DOMS) mode. *Surf Coat Technol* 2014; 258: 249–256.
- Ferreira F, Cavaleiro A and Oliveira JC. Effect of substrate biasing on the structure and properties of tantalum coatings deposited using HiPIMS in deep oscillation magnetron sputtering mode. *Metals* 2020; 10: 1618.
- Ferreira F, Oliveira JC and Cavaleiro A. CrN thin films deposited by HiPIMS in DOMS mode. *Surf Coat Technol* 2016; 291: 365–375.
- Bahr A, Glechner T, Wojcik T, et al. Non-reactive HiPIMS deposition of NbCx thin films: effect of the target power density on structure-mechanical properties. *Surf Coat Technol* 2022; 444: 128674.

32. Ataie SA, Soltanieh M, Naghizadeh R, et al. Effects of substrate temperature and reactive gas flow rate on the crystalline ceramic phases formation and tribological properties of W–Ti–Co–C–N thin films produced by co-sputtering. *Ceram Int* 2020; 46: 29137–29149.
33. Tiron V, Bulai G, Costin C, et al. Growth and characterization of W thin films with controlled Ne and Ar contents deposited by bipolar HiPIMS. *Nucl Mater Energy* 2021; 29: 101091.
34. Ferreira F, Cavaleiro A and Oliveira J. Tribological performance of DLC coatings deposited by DOMS in mixed Ar-Ne discharges. *Mater Lett* 2021; 285: 129056.
35. Boeira CD, Leidens LM, Michels AF, et al. Influence of base pressure prior to deposition on the adhesion behaviour of carbon thin films on steel. *Appl Surf Sci Adv* 2020; 2: 100034.
36. Kumada T, Ohtsuka M and Fukuyama H. Influence of substrate temperature on the crystalline quality of AlN layers deposited by RF reactive magnetron sputtering. *AIP Adv* 2015; 5: 017136.
37. Mickan M, Helmersson U and Horwat D. Effect of substrate temperature on the deposition of Al-doped ZnO thin films using high power impulse magnetron sputtering. *Surf Coat Technol* 2018; 347: 245–251.
38. Ma Q, Li L, Xu Y, et al. Effect of bias voltage on TiAl–SiN nanocomposite coatings deposited by HiPIMS. *Appl Surf Sci* 2017; 392: 826–833.
39. Ding JC, Mei H, Li Q, et al. Microstructure, mechanical and tribological properties of Mo–V–Cu–N coatings prepared by HIPIMS technique. *Ceram Int* 2022; 48: 10704–10712.
40. Ghailane A, Makha M, Larhlimi H, et al. Design of hard coatings deposited by HiPIMS and dcMS. *Mater Lett* 2020; 280: 128540.
41. Oliveira JC, Fernandes F, Serra R, et al. On the role of the energetic species in TiN thin film growth by reactive deep oscillation magnetron sputtering in Ar/N₂. *Thin Solid Films* 2018; 645: 253–264.
42. Elmkhah H, Attarzadeh F, Fattah-Alhosseini A, et al. Microstructural and electrochemical comparison between TiN coatings deposited through HIPIMS and DCMS techniques. *J Alloys Compd* 2018; 735: 422–429.
43. Wang Z, Zhang D, Ke P, et al. Influence of substrate negative bias on structure and properties of TiN coatings prepared by hybrid HIPIMS method. *J Mater Sci Technol* 2015; 31: 37–42.
44. Basu I and De Hosson JTM. Strengthening mechanisms in high entropy alloys: Fundamental issues. *Scr Mater* 2020; 187: 148–156.
45. Koutzaki SH, Krzanowski JE and Nainaparampil JJ. Phase formation and microstructure in sputter-deposited Ti–Mo–C and Ti–WC thin films. *Metall Mater Trans A* 2002; 33: 1579–1588.
46. Hovsepian PE, Sugumaran AA, Purandare Y, et al. Effect of the degree of high power impulse magnetron sputtering utilisation on the structure and properties of TiN films. *Thin Solid Films* 2014; 562: 132–139.